

## Coulomb Milne problem

J. Barrett,\* L. Demeio, and B. Shizgal†

*Department of Chemistry, University of British Columbia, Vancouver, British Columbia, Canada*

(Received 27 August 1991)

The transport properties of an ensemble of charged test particles diffusing from infinity through a second charged species that fills the positive half-space are studied. It is assumed that there are no incoming particles at the boundary between the medium in the positive half-space and the vacuum that fills the negative half-space. This problem has been referred to as the Milne problem and has previously been considered for neutral species [M. J. Lindenfeld and B. Shizgal, *Phys. Rev. A* **27**, 1657 (1983)]. The present paper examines the rarefied-gas dynamical effects for the Coulomb interaction between the two species. The distribution function of the background gas is taken to be a Maxwellian and the test-particle distribution is determined from a solution of the Boltzmann equation with its expansion in Burnett functions, products of Laguerre polynomials, and spherical harmonics. The extrapolation length is calculated together with the density and temperature profiles and compared with the Chapman-Enskog results valid far from the boundary. A comparison with the previous results for the hard-sphere cross section describing collisions between two neutral species is also presented.

PACS number(s): 51.10.+y, 05.20.Dd, 05.60.+w

## I. INTRODUCTION

The Milne problem refers to the diffusion of a minor constituent of test particles through a background species considered to be at equilibrium. The background species occupies the half-space  $r > 0$  whereas a vacuum exists in the half-space  $r \leq 0$ . Figure 1 shows the physical problem that we are considering. A current density of magnitude  $\bar{j}$  directed in the negative- $r$  direction exists in the medium and it is assumed that there are no other sinks or sources of particles within the medium, but the plane at  $r = 0$  is an absorbing boundary. The problem consists of determining the steady velocity distribution of the minor species within the half-space of interest and at the boundary.

This model was first considered by Milne [1] for the transport of photons and the study of the steady intensity of radiation in the interior of a star and the emergent angular distribution. The test particles can also be neutrons diffusing through a reactor in which case the steady neutron velocity distribution function is the desired quantity. The relationship between the neutron transport and the radiative transport problems has been presented in detail by Kourganoff [2]. The Milne problem has a very long history and has been described in standard texts [3]. A detailed theoretical analysis of the Milne problem for neutral minor and major constituents interacting via a hard-sphere cross section was presented several years ago by Lindenfeld and Shizgal [4], referred to as paper I. The departure from an equilibrium Maxwellian distribution function arises from the imposition of a constant flux at infinity directed towards the negative- $r$  direction and the condition that there are no particles incident from the left. The velocity distribution function of the minor diffusing species is assumed to be given by the Boltzmann equation subject to these boundary conditions. The basic objective of this work was the study of the rarefied-gas

dynamical effect that occurs near the boundary with the vacuum and the range of validity of hydrodynamics in the vicinity of the boundary. The main emphasis of this earlier paper was the study of the range of validity of Fick's law of diffusion, that is,

$$\bar{J} = -\bar{D} d\bar{n}(r)/dr, \quad (1)$$

where  $\bar{n}(r)$  is the number density of the minor species and  $\bar{D}$  is the diffusion coefficient. The overbar is used to denote dimensional quantities and is omitted for dimensionless variables defined later. Far from the boundary, the density profile can be determined from Fick's law and varies linearly with distance, whereas close to the boundary (within a mean free path) the density profile is curved. The extrapolation of the asymptotic linear density profile in the negative- $r$  direction intercepts the  $r$  axis on the negative side by some amount  $q$  referred to as the extra-

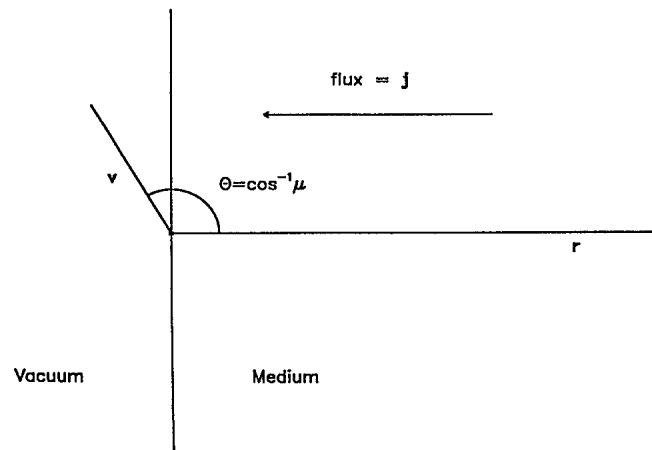


FIG. 1. Geometry of the Milne problem.

polation length [3]. The method of solution of the Boltzmann equation is based on the expansion of the distribution function in Burnett functions which are products of Laguerre polynomials in the particle energy and spherical harmonic functions for the orientation of the particle velocity as employed by Frankowski, Alterman, and Pekeris [5] in their study of heat conduction.

Recently, Loyalka, Hamoodi, and Tompson [6] considered a similar model to describe the isothermal condensation of a vapor diffusing through a background gas. They considered planar geometry and a hard-sphere interaction and with the  $S_N$  method of solution of the transport equation [7] obtained agreement with Lindenfeld and Shizgal [4] for the extrapolation length or jump distance. Similar models but with Fokker-Planck-type collision operators were considered by Razi Naqvi, Waldenstrom, and Mork [8], Waldenstrom, Mork, and Razi Naqvi [9], and by Sahni [10]. Sahni employed the method of solution introduced by Lindenfeld and Shizgal but considered spherical geometry in place of the planar geometry of Fig. 1. Only a small number of terms in the Burnett function expansion was used. A half-range expansion was considered by Razi Naqvi, Waldenstrom, and Mork [8] and Waldenstrom, Mork, and Razi Naqvi [9], and a summary of the half-range versus the full-range treatments was presented recently by Razi Naqvi, Mork, and Waldenstrom [11]. There is some overlap of the moment methods used by these authors and the present paper, with moment methods employed by Johnson [12] in connection with sound waves in disparate-mass-gas mixtures. Also, there has been considerable work by Titulaer and co-workers [13] on the related Klein-Kramers equation and on the linear Bhatnagar-Gross-Krook equation.

A Monte Carlo study of the Milne problem in planar geometry was recently presented by Barakat and Lemaire [14]. They considered a solution of the Milne problem for both hard spheres and the Maxwell molecule interaction, for which they assumed isotropic scattering and did not employ the rigorous differential elastic cross section. The calculation of the extrapolation length is somewhat awkward with the Monte Carlo method, as the asymptotic linear portion of the density profile in the continuum region is not unambiguously identified. Barakat and Lemaire also considered the analogous problem of the escape of a light atmospheric constituent from a planetary atmosphere and compared with results obtained by Shizgal and Blackmore [15]. The relationship of the Milne problem and the escape of atmospheres has been discussed by Fahr and Shizgal [16]. In this situation, the diffusing particles leave the medium, that is the atmosphere, only if their speed exceeds the escape speed for the planet.

The purpose of the present paper is to apply the formalism of paper I to a binary system of charged species interacting via the Coulomb cross section. We are interested in the rarefied-plasma dynamical effects that occur within a mean-free path of the boundary between the medium and the vacuum. A comparison with the results in I for the hard-sphere cross section is of interest. There are many ionized systems for which the Chapman-Enskog method for the determination of trans-

port coefficients [17]–[19] and the usual linear transport equations are no longer valid. These include the supersonic expansion of the solar atmosphere referred to as the solar wind [20], transport processes in the high altitude ionosphere [21], heat conduction in the interstellar gas, and in laser plasma fusion [22,23]. The diffusion of charged particles in collisional plasmas in connection with space-charge effects in gas discharges has recently been reviewed by Phelps [24].

In all these situations the length scale of the inhomogeneities in the system is of the same order as the mean-free path. A reduction in the heat flux in the solar wind has been recognized long ago and remains an important unsolved theoretical problem [25]. Moreover, there has been considerable interest in the study of the breakdown of Fourier's law of heat transport

$$\bar{Q} = -\bar{\lambda} d\bar{T}(r)/dr, \quad (2)$$

where  $\bar{\lambda}$  is the heat conductivity and  $\bar{T}(r)$  is the temperature. The heat conductivity is generally determined with the Chapman-Enskog [19] method of solution of the Boltzmann or Fokker-Planck equations. This approach assumes that the plasma is collision dominated or that the Knudsen number  $Kn = l/L$  (the ratio of the mean-free path to a length scale characteristic of the system inhomogeneity), is very much less than unity. Anomalous transport has been considered by Luciani, Mora, and Pellet [26] with a model Fokker-Planck equation. Belyi, Demoulin, and Paiva-Veretennicoff [27] considered a solution of the Fokker-Planck equation with a modification of Grad's 13-moment method [28].

The physical situation considered in this work, Fig. 1, with the background gas in large excess and taken to be at equilibrium does not allow for a heat flux as given by Eq. (2) as the temperature of the mixture reduces to the temperature of the bath which is constant. It is common for many nonequilibrium situations [21], [29] and [30] to relate the heat transported by each component in a mixture to the temperature gradients of each species which are not necessarily equal. We will show that for this system the heat flux of the test-particle species  $\bar{Q}_1$  is not proportional to  $d\bar{T}_1/dr$  in the region far from the boundary. Rather we find that the heat flux is proportional to the density gradient and the transport coefficient is a modified thermal-diffusion coefficient [32,33].

The present paper follows the methodology introduced in paper I. The distribution function is written as a sum of a spatial transient and asymptotic parts. The spatial transient portion of the solution plays an important role near the boundary whereas the asymptotic solution dominates in the region far from the boundary. An expansion in Burnett functions is employed to determine the distribution function in velocity and spatial coordinates. The solution provides the density and temperature profiles and the linear phenomenological transport equations are tested. The present work is also an outgrowth of the interest of one of the authors in the thermal escape of charged particles from high latitudes of the terrestrial atmosphere. The escape of protons and  $\text{He}^+$  ions from the topside ionosphere (approximately 1500 km) is referred to as the polar wind in analogy with the supersonic solar

wind expansion [16]. This problem (for a plane-parallel atmosphere) is similar to the present Milne problem, although the external gravitational and (self-consistent) polarization potential must be included. A discussion of the method of solution of the Boltzmann equation for a plane-parallel atmosphere based on the half-range expansion as suggested by Razi Naqvi, Mork, and Waldenstrom [11] was published earlier by Shizgal, Weinert, and Lemaire [34]. It is anticipated that the methods of solution of the Fokker-Planck equation used here and in paper I will prove useful in the atmospheric escape problem.

Section II of the paper contains a brief discussion of the Fokker-Planck equation for the Coulomb Milne problem and the division of the solution into spatial transient and asymptotic portions. The results of the numerical calculations and their discussion are presented in Sec. III.

$$\bar{J}[\bar{f}] = \frac{\mathcal{C}}{m} \frac{\partial}{\partial \mathbf{v}} \cdot \int \frac{u^2 |-\mathbf{u}\mathbf{u}|}{u^3} \cdot \left[ \frac{1}{m} \bar{f}_1^M(\mathbf{v}') \frac{\partial \bar{f}(\mathbf{v})}{\partial \mathbf{v}} - \frac{1}{m_1} \bar{f}(\mathbf{v}) \frac{\partial \bar{f}_1^M(\mathbf{v}')}{\partial \mathbf{v}'} \right] d\mathbf{v}', \quad (4)$$

where  $\mathcal{C} = 2\pi Z^2 Z_1^2 \ln \Lambda$  with  $Z$  and  $Z_1$  the charges of the test particle and heat-bath particle, respectively,  $\ln \Lambda$  the Coulomb logarithm,  $\mathbf{u} = \mathbf{v} - \mathbf{v}'$  and  $\mathbf{I}$  is the unit tensor. Equation (4) is the Landau form of the collision operator which only takes into account large-impact-parameter collisions [19]. The range of validity of this form of the collision operator has been discussed by Shoub [35]. With the definition of an effective hard-sphere cross section,  $\sigma_{\text{eff}} = \mathcal{C} / (2kT)^2$ , and the transformation to dimensionless variables,  $x = \sigma_{\text{eff}} \int_0^r \bar{n}_1(r') dr'$ ,  $J = \bar{J} / (\sigma_{\text{eff}} v_0)$ ,  $f = \bar{f} [v_0 / \bar{n}_1(r) \sigma_{\text{eff}}]^3$ , the Fokker-Planck equation can be written in the form,

$$p\mu \frac{\partial f(x, p, \mu)}{\partial x} = J(f(x, p, \mu)). \quad (5)$$

We seek solutions of this equation subject to the boundary condition that no particles in the negative  $x$  region return to the medium, that is,

$$f(0, p, \mu) = 0, \quad 0 < \mu < 1. \quad (6)$$

The method of solution of the Boltzmann equation for the hard-sphere cross section was described in detail in I. Therefore, we provide here a very brief outline of the formalism and the changes that arise from the use of the Coulomb cross section in this paper. The general solution is written as the sum of the spatial transient part  $f^{\text{tran}}$  and an asymptotic part  $f^{\text{asympt}}$ , that is,

$$f = f^{\text{tran}} + f^{\text{asympt}}. \quad (7)$$

The transient solution dominates near the  $x = 0$  boundary and decays out in a distance of the order of a few mean free paths. The asymptotic solution dominates at large distances where hydrodynamics is expected to be valid.

It was shown in I that the transient solution is of the form,

$$f^{\text{tran}}(x, p, \mu) = \sum_{k=0}^{\infty} a_k e^{g_k x} R_k(p, \mu), \quad (8)$$

## II. SOLUTION OF THE FOKKER-PLANCK EQUATION

For steady-state conditions the Fokker-Planck equation for the velocity distribution function of test ions  $\bar{f}(r, v, \mu)$  is,

$$v\mu \frac{\partial \bar{f}(r, v, \mu)}{\partial r} = \bar{n}_1(r) \bar{J}(\bar{f}(r, v, \mu)), \quad (3)$$

where  $\mu = \cos(\theta)$  and  $\theta$  is the angle between  $\mathbf{v}$  and the positive  $r$  axis as shown in Fig. 1. In Eq. (3),  $\bar{n}_1(r)$  is the number density of the background medium, which is assumed to be characterized by a Maxwellian distribution function,  $\bar{f}_1^M = (m/2\pi kT)^{1/2} \exp(-p^2)$  where  $p = v/v_0$  and  $v_0^2 = 2kT/m$ . With these definitions, the linear Fokker-Planck collision operator for Coulomb collisions is given by [19]

where  $g_k$  and  $R_k(p, \mu)$  are the spatial eigenvalues and eigenfunctions, respectively, given by,

$$J[R_k] = (p\mu) g_k R_k. \quad (9)$$

The eigenfunctions and eigenvalues are determined with the expansion of  $R_k$  in Burnett functions  $\psi_{nl}(p, \mu)$

$$R_k(p, \mu) = \frac{\exp(-p^2)}{\pi^{3/2}} \sum_{n=0}^{\infty} \sum_{l=0}^{\infty} b_{nl}^k \psi_{nl}(p, \mu). \quad (10)$$

The Burnett functions are products of spherical harmonics and Laguerre polynomials and are defined by Eqs. (2.12)–(2.15) of I. The eigenvalue problem is then converted to the finite set of linear equations,

$$\sum_{n'=0}^N \sum_{l'=0}^L (A_{nl, n'l'} - g_k B_{nl, n'l'}) b_{n'l'}^k = 0, \quad (11)$$

where  $A_{nl, n'l'}$  are the matrix elements of the Fokker-Planck collision operator calculated as described by Wong [36] in a recent paper. The  $B_{nl, n'l'}$  quantities are the matrix elements of  $p\mu$  as discussed in I and given explicitly by Eq. (2.20) of that paper. Numerical diagonalization of the matrix in Eq. (11) gives approximate eigenvalues and eigenfunctions to order  $K = (N+1)(L+1)$ . As discussed in I and in the work by Frankowski, Alterman, and Pekeris [5], the eigenvalues  $g_k$ , which include the zero eigenvalue, occur in positive and negative pairs so that the sum over  $k$  in Eq. (8) includes only nonzero negative  $g_k$ . The transient solution is then written as

$$f^{\text{tran}}(x, p, \mu) = \sum_{k=1}^{1/2K-1} a_k e^{g_k x} R_k(p, \mu), \quad (12)$$

and the asymptotic solution is written in the form

$$f^{\text{asympt}}(x, p, \mu) = -(j/D) f^M(p) [q + x - \mu U(p)], \quad (13)$$

where the dimensionless flux and diffusion coefficient are given by  $j = \bar{j} / v_0 [\bar{n}_1(r) \sigma_{\text{eff}}]^3$  and  $D = \bar{D} / [v_0 / \bar{n}_1(r) \sigma_{\text{eff}}]$ ,

respectively. The function  $U(p)$  satisfies the Chapman-Enskog equation for diffusion [17], that is,

$$I(\mu U(p)) = -p\mu, \quad (14)$$

and is solved with the expansion

$$\mu U(p) = \sum_{n'=0}^{\infty} d_{n'} \psi_{n'}(p, \mu). \quad (15)$$

Consequently, the solution of Eq. (14) is given by

$$\sum_{n'=0}^{\infty} A_{n1, n'} d_{n'} = -\delta_{n0}/\sqrt{2}, \quad (16)$$

and the diffusion coefficient is given by

$$D = d_0/\sqrt{2}. \quad (17)$$

The general solution is written with the substitution of Eq. (10) into Eq. (8) and combined with (13) giving Eq. (2.32) of I. The  $b_{nk}$  coefficients are determined by the eigenvalue problem, Eq. (11) whereas the  $a_k$  coefficients and the extrapolation length  $q$  are calculated from the boundary conditions. This aspect of the calculation has been discussed at great length in I and is not repeated here. It is sufficient to note that there are several different choices for the imposition of the boundary conditions. As done in the previous paper we here consider the Marshak and variational boundary conditions. In this way, the distribution function and the extrapolation length are determined.

### III. RESULTS AND DISCUSSION

The distribution function is calculated by setting up the matrices **A** and **B**, solving the eigenvalue problem, Eq. (11), the set of linear equations, Eq. (16), and applying the Marshak and variational boundary conditions, Eq. (3.1) and (3.7) which lead to Eqs. (3.6) and (3.8) of I. The

important quantities in this study are the spatial eigenvalues,  $g_k$ , that determine the rate of the decay of the transient solution with increasing  $x$ , the extrapolation length,  $q$ , and, in particular, the density and temperature profiles of the diffusing species. These quantities depend on the mass ratio of minor and major constituents,  $\gamma = m_1/m$ , and the number of basis functions used in the solution of the Boltzmann equation. It is not known whether the eigenvalue spectrum of the spatial eigenvalues is discrete or continuous. Nevertheless we show the rate of convergence of the four lower-order eigenvalues versus the indices  $L$  and  $N$  for several values of the mass ratio  $\gamma$  in Tables I–IV. As can be seen, when  $\gamma$  is very small (Tables I and II) the convergence is rapid versus  $N$  and  $L$ . For  $\gamma = 0.01$  in Table I, the four eigenvalues shown have converged to three significant figures to the order of the solutions shown. In Table II, for  $\gamma = 0.03$ , only the first two eigenvalues have converged. With increasing  $\gamma$ , although the number of Legendre polynomials decreases, there is no convergence for any eigenvalue to the maximum order  $N$  shown in tables, as can be seen from the result for  $\gamma = 10$  in Table IV. This is not unexpected since the discrete spectrum of the Fokker-Planck collision operator for the relaxation of an isotropic distribution function is empty [37], although there are several pseudodiscrete eigenvalues as reported by Shizgal [38]. If the eigenfunctions belong to the continuous spectrum, then their calculation with an expansion in a finite basis set is not expected to be convergent.

The nonconvergence of the eigenvalues does not detract from the present method of solution since the important physical quantities, that are averages of the distribution function, converge as we show. A detailed explanation for the convergence of the averaged quantities despite the nonconvergence of the eigenvalues is provided in [38]. For example, the convergence of the extrapolation length is shown for four different values of  $\gamma$  in

TABLE I. Convergence of spatial eigenvalues;  $\gamma = 0.01$ .

$N$	$L$	6	8	10	12
First eigenvalue					
6		0.2064	0.2059	0.2059	
8		0.2064	0.2059	0.2059	
Second eigenvalue					
6		0.2855	0.2830	0.2824	0.2824
8		0.2851	0.2826	0.2820	0.2820
10		0.2851	0.2826	0.2820	0.2820
Third eigenvalue					
6		0.3099	0.2920	0.2903	0.2902
8		0.3097	0.2920	0.2902	0.2902
10		0.3097	0.2920	0.2902	0.2902
Fourth eigenvalue					
6		0.3586	0.3484	0.3442	0.3420
8		0.3441	0.3370	0.3353	0.3350
10		0.3428	0.3359	0.3343	0.3340
12		0.3427	0.3358	0.3343	0.3339

TABLE II. Convergence of spatial eigenvalues;  $\gamma=0.03$ .

$N \backslash L$	6	8	10	12
First eigenvalue				
6	0.3331	0.3323	0.3323	
8	0.3331	0.3323	0.3323	
Second eigenvalue				
6	0.4320	0.4261	0.4248	0.4248
8	0.4256	0.4199	0.4187	0.4186
10	0.4243	0.4185	0.4173	0.4172
12	0.4240	0.4181	0.4168	0.4166
14	0.4238	0.4178	0.4163	0.4160
16	0.4236	0.4166	0.4119	0.4082
Third eigenvalue				
6	0.4990	0.4668	0.4616	0.4609
8	0.4852	0.4665	0.4610	0.4600
10	0.4660	0.4560	0.4519	0.4502
12	0.4545	0.4439	0.4395	0.4376
14	0.4446	0.4329	0.4277	0.4250
16	0.4327	0.4207	0.4176	0.4170
Fourth eigenvalue				
6	0.5417	0.5151	0.5010	0.4952
8	0.5026	0.4754	0.4703	0.4684
10	0.4998	0.4665	0.4610	0.4602
12	0.4922	0.4665	0.4610	0.4601
14	0.4739	0.4617	0.4546	0.4478
16	0.4598	0.4477	0.4406	0.4328

TABLE III. Convergence of spatial eigenvalues;  $\gamma=1.0$ .

$N \backslash L$	6	8	10	12
First eigenvalue				
6	0.08961	0.08939	0.08939	
8	0.05969	0.05954	0.05953	
10	0.04411	0.04397	0.04397	
12	0.03470	0.03458	0.03457	
16	0.02406	0.02395	0.02394	
Second eigenvalue				
6	0.1302	0.1205	0.1193	0.1192
8	0.08488	0.07931	0.07861	0.07857
10	0.06126	0.05770	0.05720	0.05718
12	0.04701	0.04467	0.04430	0.04428
16	0.03113	0.03007	0.02983	0.02982
Third eigenvalue				
6	0.1900	0.1680	0.1530	0.1495
8	0.1074	0.1018	0.09814	0.09712
10	0.07296	0.06944	0.06833	0.06810
12	0.05467	0.05165	0.05104	0.05095
16	0.03600	0.03339	0.03299	0.03295
Fourth eigenvalue				
6	0.2320	0.1936	0.1873	0.1812
8	0.1364	0.1164	0.10890	0.1072
10	0.09167	0.08189	0.07630	0.07490
12	0.06681	0.06172	0.05816	0.05711
16	0.04125	0.03949	0.03834	0.03777

TABLE IV. Convergence of spatial eigenvalues;  $\gamma = 10$ .

$N \backslash L$	6	8	10	12
First eigenvalue				
6	0.01686	0.01686		
8	0.01025	0.01025		
10	0.00713	0.00713		
12	0.00537	0.00537		
16	0.00350	0.00350		
Second eigenvalue				
6	0.03657	0.03656		
8	0.01814	0.01814		
10	0.01135	0.01135		
12	0.00797	0.00797		
16	0.00476	0.00476		
Third eigenvalue				
6	0.05306	0.05257	0.05257	
8	0.02881	0.02868	0.02868	
10	0.01747	0.01745	0.01745	
12	0.01156	0.01156		
16	0.00634	0.00634		
Fourth eigenvalue				
6	0.09985	0.08847	0.08644	0.08635
8	0.03621	0.03600	0.03599	
10	0.02079	0.02064	0.02064	
12	0.01435	0.01425	0.01425	
16	0.00815	0.00812	0.00812	

Tables V–VIII. Although the calculations have to be carried out to fairly high order ( $N, L \approx 12$ ), the extrapolation length has converged to three significant figures. The rate of convergence appears to be almost independent of the mass ratio.

In Fig. 2, we show the extrapolation length as function of  $\gamma$  in comparison with the behavior for the hard-sphere

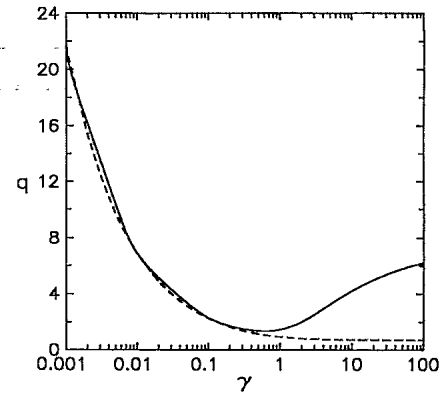


FIG. 2. Extrapolation length  $q$  vs  $\gamma$  for the Coulomb cross section (solid line) and for the hard-sphere cross section (dashed line).

cross section (dashed curve). The behavior appears to be very similar up to  $\gamma \approx 1$ , but the two curves deviate significantly for larger mass ratios. In particular, the extrapolation length for the Coulomb case has a minimum at  $\gamma \approx 0.6$  and increases for increasing  $\gamma$ . Evidently, the details of the cross section is more sensitive in the Lorentz limit ( $\gamma \rightarrow \infty$ ) than in the Rayleigh limit ( $\gamma \rightarrow 0$ ).

The different behavior of the extrapolation length for the two cross sections is also shown in terms of the actual density profiles of the diffusing particles and calculated with the solution of the Boltzmann equation as given by Eq. (4.6) of I,

$$n(x) = \int f(x, p, \mu) dp = \sum_{k=1}^{1/2K-1} a_k e^{g_k x} b_{00}^k + D^{-1}(q+x). \tag{18}$$

In Fig. 3, the density profile in the case of the Coulomb cross section is shown for three different values of  $\gamma$  (compare with Fig. 6 of I, where the density profiles are

TABLE V. Convergence of the extrapolation length;  $\gamma = 0.1$ .

$N \backslash L$	2	4	6	8	10	12
Marshak boundary conditions						
2	2.108	2.270	2.279	2.279		
4	2.123	2.290	2.300	2.302		
6	2.125	2.293	2.305	2.307	2.308	
8		2.294	2.307	2.309	2.310	2.310
10				2.310	2.311	2.311
12				2.311	2.312	2.312
Variational boundary condition						
2	1.553	2.091	2.124	2.128		
4	1.585	2.159	2.205	2.212	2.213	
6	1.591	2.177	2.230	2.241	2.244	
8	1.593	2.184	2.242	2.256	2.260	
10		2.187	2.248	2.264	2.269	
12			2.252	2.270	2.276	2.278

TABLE VI. Convergence of the extrapolation length;  $\gamma=0.2$ .

$N \backslash L$	2	4	6	8	10	12
Marshak boundary conditions						
2	1.591	1.718	1.724	1.725		
4	1.605	1.734	1.741	1.743		
6	1.607	1.736	1.745	1.747		
8			1.746	1.748		
10			1.747	1.749	1.750	1.750
12				1.750	1.750	1.750
Variational boundary condition						
2	1.178	1.585	1.607	1.609		
4	1.202	1.636	1.669	1.673		
6	1.207	1.650	1.689	1.697	1.698	
8	1.208	1.655	1.698	1.708	1.711	
10			1.703	1.715	1.719	
12			1.706	1.719	1.723	1.725

shown for the hard-sphere cross section). The dashed lines represent the asymptotic linear dependence in the hydrodynamic regime far from the wall given by Eq. (2.25) of I,

$$n_{\text{asympt}}(x) = -\frac{j}{D}(q+x). \quad (19)$$

The extrapolation lengths for curve  $a$  ( $\gamma=0.2$ ) and curve  $c$  ( $\gamma=5$ ) inferred from these results are nearly equal and larger than the one for curve  $b$  ( $\gamma=1$ ), consistent with the results in Fig. 2. This behavior is further demonstrated in Figs. 4(a) (Coulomb) and 4(b) (hard sphere) for  $\gamma=50$ , and similarly in Figs. 4(c) (Coulomb) and 4(d) (hard sphere) for  $\gamma=0.01$ . The dashed line is the asymptotic density profile and is shown here extrapolated to the negative  $x$  axis so as to show the different values of the extrapolation length. The behavior in the upper pair of graphs for the large mass ratio is different whereas it is very simi-

lar in the lower pair of figures with the smallest mass ratio.

One of the main interests in the present paper is the study of the rate of decay of the transient solution near the boundary. The particle flux expressed as  $D dn/dx$  is shown in Figs. 5(a) and 5(b) for the Coulomb cross section and the hard-sphere cross section, respectively. In the hydrodynamic region ( $x \rightarrow \infty$ ),  $D dn/dx \rightarrow 1$ , consistent with the chosen normalization. Whereas the rate of decay of the spatial transients for the hard-sphere cross section [Fig. 5(b)] decreases monotonically with mass ratio, the behavior for the Coulomb cross section [Fig. 5(a)] is consistent with the minimum obtained for the extrapolation length in Fig. 2. The result for  $\gamma=0.1$  (curve  $a$ ) lies between the results for the other two mass ratios.

Near the boundary at  $x=0$  the temperature of the test particles can be different from the temperature of the bath in contrast to the usual Chapman-Enskog treatment

TABLE VII. Convergence of the extrapolation length;  $\gamma=1$ .

$N \backslash L$	2	4	6	8	10	12
Marshak boundary conditions						
2	1.233	1.382	1.370	1.371		
4	1.333	1.460	1.467	1.468	1.468	
6	1.336	1.463	1.469	1.470	1.471	
8			1.470	1.471	1.472	
10				1.472	1.472	1.473
12				1.472	1.473	1.473
Variational boundary condition						
2	0.950	1.285	1.300	1.299	1.298	
4	1.039	1.399	1.422	1.425	1.425	
6	1.042	1.407	1.434	1.440	1.442	
8		1.410	1.440	1.447	1.450	
10				1.451	1.454	1.455
12				1.453	1.457	1.458

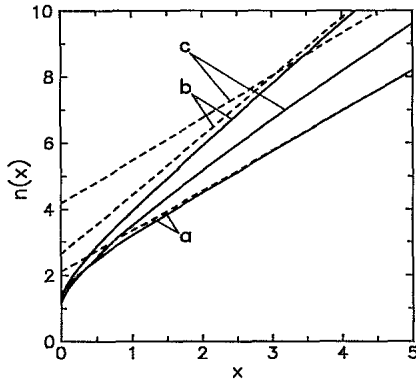


FIG. 3.  $n(x)$  (solid lines) and  $n_{\text{asympt}}(x)$  (dashed lines) vs  $x$  for (curve *a*)  $\gamma=0.2$ , (curve *b*)  $\gamma=1$ , and (curve *c*)  $\gamma=5$  for the Coulomb cross section.

of a gas mixture [17]. The spatial decay of the temperature of the test particle,  $T(x)/T_1$ , is shown in Fig. 6 with the Coulomb cross section in the upper graph and the hard-sphere cross section in the lower graph. For the hard-sphere case, the temperature of the test particles is everywhere less than the temperature of the background gas. This might have been interpreted as a cooling of the test particles near the boundary owing to their loss from the system. However, for the Coulomb cross section (upper graph) we find that for the large mass ratios there is a heating of the test particles in a small region near the boundary followed by a slow approach to the bath temperature.

The heat flux carried by the test particles is a manifestation of thermal diffusion rather than Fourier's law [Eq. (2)] referred to the test-particle species. The heat flux is given by

$$Q(x) = \int p^3 \mu f(x, p, \mu) dp$$

$$= \frac{\sqrt{5}}{2} \left[ \sum_k a_k e^{g_k x} (\sqrt{\frac{5}{2}} b_{01}^k - b_{11}^k) - \sqrt{5} + \frac{d_1}{D} \right] \quad (20)$$

and the asymptotic heat flux is

$$Q_{\text{asympt}} = \int p^3 \mu f^{\text{asympt}}(x, p, \mu) dp$$

$$= \frac{1}{D} \left[ \frac{d_1}{N_{11}} - \frac{5}{2} \frac{d_0}{N_{01}} \right]. \quad (21)$$

The ratio of the heat flux relative to the asymptotic value is shown in Fig. 7 for both cross sections for several mass ratios. For the hard-sphere cross section shown in the lower graph [7(b)] this ratio appears to decrease monotonically with increasing mass ratio from curve *a* to curve *c*. At mass ratio  $\gamma \approx 5$  the derivative  $d(Q/Q_{\text{asympt}})/dx$  at the origin changes sign. By contrast,  $Q/Q_{\text{asympt}}$  for the Coulomb cross section, shown in the upper graph [7(a)], decreases with  $x$  for all mass ratios. It is useful to note that for mass ratio  $\gamma=10$  (curve *c*)  $Q(x)/Q_{\text{asympt}}$  appears to be nonmonotonic. In Fig. 8, we show the ratios  $Q/(dn/dx)$  and  $Q/(dT/dx)$  and it is clear that whereas

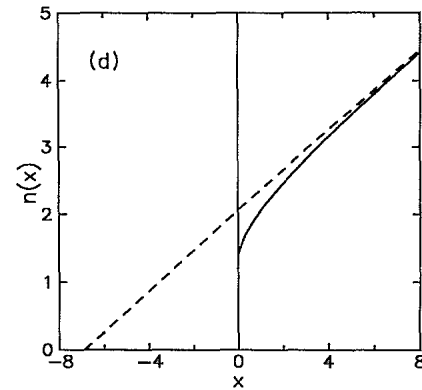
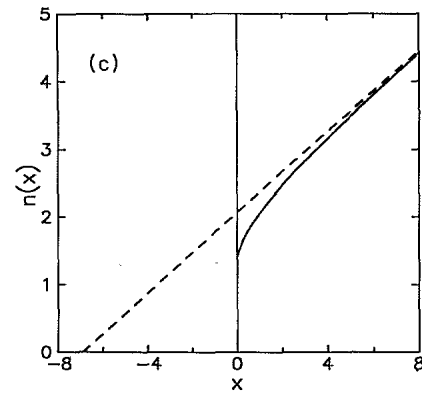
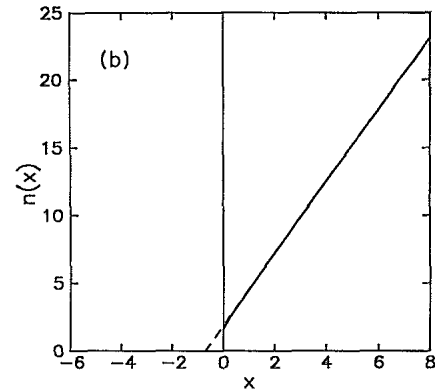
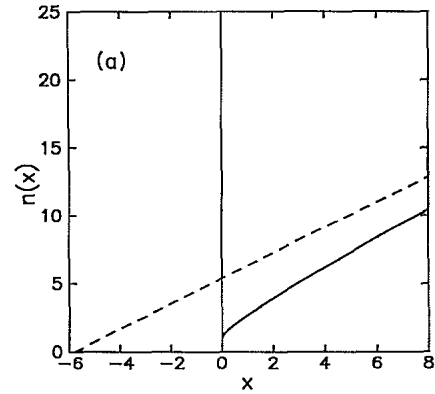


FIG. 4.  $n(x)$  (solid lines) and  $n_{\text{asympt}}(x)$  (dashed lines) vs  $x$  for (a) the Coulomb cross section and  $\gamma=50$ ; (b) the hard-sphere cross section and  $\gamma=50$ ; (c) the Coulomb cross section and  $\gamma=0.01$ ; (d) the hard-sphere cross section and  $\gamma=0.01$ .

TABLE VIII. Convergence of the extrapolation length;  $\gamma=10$ .

$N \backslash L$	2	4	6	8	10	12
Marshak boundary conditions						
2	2.935	3.246	3.266	3.271	3.273	
4	3.860	4.167	4.185	4.190	4.191	
6	3.885	4.183	4.201	4.206	4.208	
8	3.889	4.186	4.203	4.208	4.210	4.211
10				4.209	4.211	4.212
12				4.210	4.211	4.212
Variational boundary condition						
2	2.324	3.143	3.198	3.207	3.206	3.204
4	3.134	4.055	4.127	4.150	4.158	4.161
6	3.150	4.070	4.146	4.171	4.181	4.185
8	3.153	4.073	4.149	4.175	4.186	4.191
10	3.154	4.074	4.151	4.177	4.188	4.194
12		4.075	4.152	4.178	4.190	4.195

the first ratio tends to a constant as  $x \rightarrow \infty$ , the second ratio continues to vary with  $x$ . This shows that the asymptotic heat flux is proportional to the density gradient of the test-particle species rather than to the temperature gradient and is therefore due entirely to thermal diffusion. We write in this case

$$Q_{\text{asympt}} = -\kappa \frac{dn_{\text{asympt}}}{dx}, \quad (22)$$

where  $\kappa$  is the thermal diffusion ratio. Far from the boundary, where hydrodynamics holds, the heat flux is

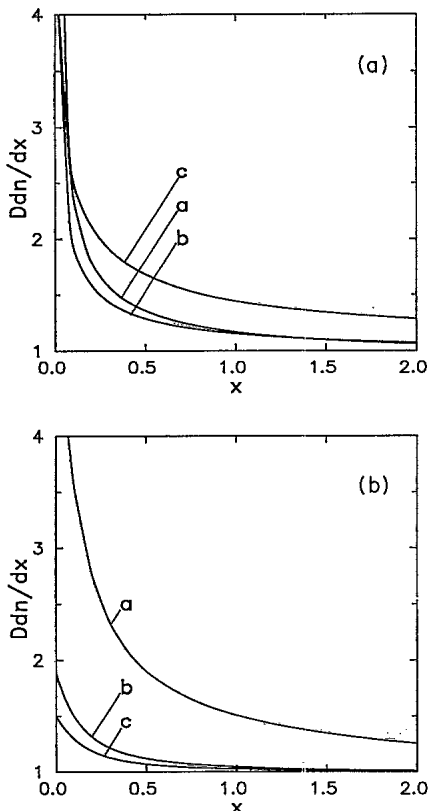


FIG. 5.  $D dn/dx$  vs  $x$  for (a) the Coulomb cross section and (b) the hard-sphere cross section and (curve a),  $\gamma=0.1$ ; (curve b),  $\gamma=1$ ; and (curve c),  $\gamma=10$ .

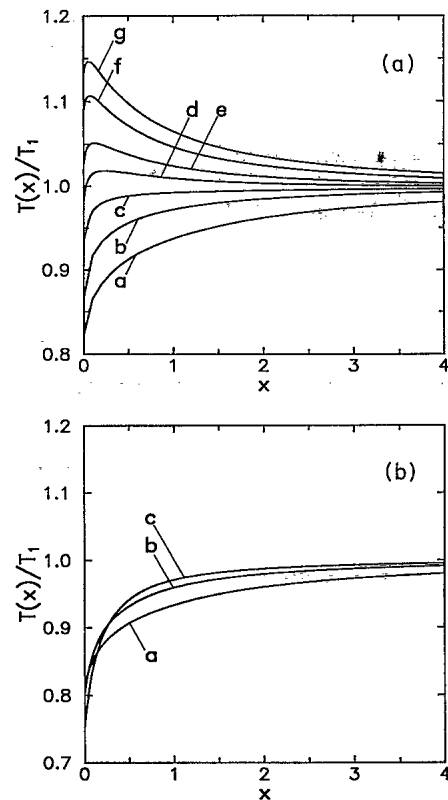


FIG. 6. Temperature profiles  $T(x)/T_1$  vs  $x$  for (a) the Coulomb cross section and (curve a),  $\gamma=0.1$ ; (curve b),  $\gamma=0.5$ ; (curve c),  $\gamma=1$ ; (curve d),  $\gamma=2$ ; (curve e),  $\gamma=3$ ; (curve f),  $\gamma=4$ ; and (curve g),  $\gamma=4.5$  and (b) the hard-sphere cross section and (curve a),  $\gamma=0.1$ ; (curve b),  $\gamma=0.5$ ; and (curve c),  $\gamma=4.5$ .

expected to agree with the one predicted by the Chapman-Enskog (CE) theory for binary gas mixtures. As mentioned earlier, Eq. (14) of the present work is the CE equation for diffusion. This integral equation is solved by expanding the distribution function in Burnett functions as done in the CE approach. If this expansion is carried to first order, analytic results for the distribution and the transport coefficients are obtained. The formalism in Sec. II permits a solution of the integral equation to higher order.

Thermal diffusion has received considerable attention in the literature [32,33,39]. The thermal-diffusion ratio (or the thermal-diffusion coefficient) depends upon the densities of the two components  $n_1$  and  $n_2$ , the temperature of the mixture  $T$ , and the cross sections for collisions of the two species with themselves (1-1 and 2-2 collisions) and with each other (1-2 collisions). Here, we take species 2 as the test particles and species 1 as the moderator. If the two components have different temperatures  $T_1$  and  $T_2$  (as we observe in the present problem) determined from the mean energies then the definition of the temperature of the mixture is

$$T = \frac{n_1 T_1 + n_2 T_2}{n_1 + n_2} \quad (23)$$

The physical system considered here pertains to a binary

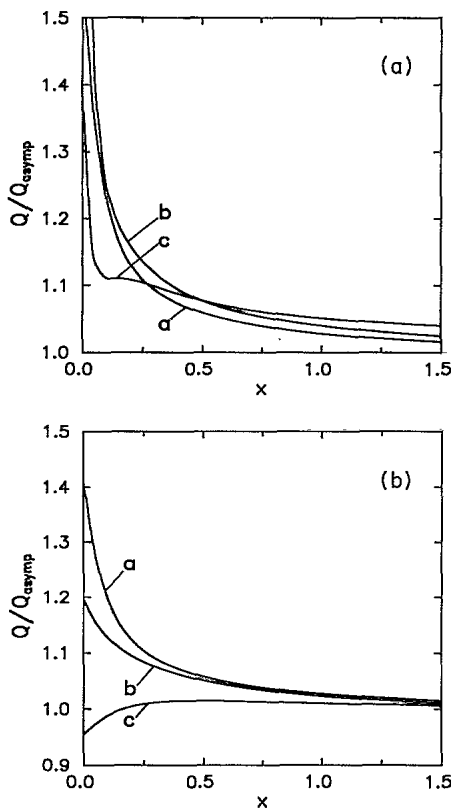


FIG. 7. Ratio of the actual heat flux  $Q(x)$  to the asymptotic (Chapman-Enskog) heat flux  $Q_{asymp}$  for (a) the Coulomb cross section and (b) the hard-sphere cross section and (curve a),  $\gamma=0.1$ ; (curve b),  $\gamma=1$ ; and (curve c),  $\gamma=10$ .

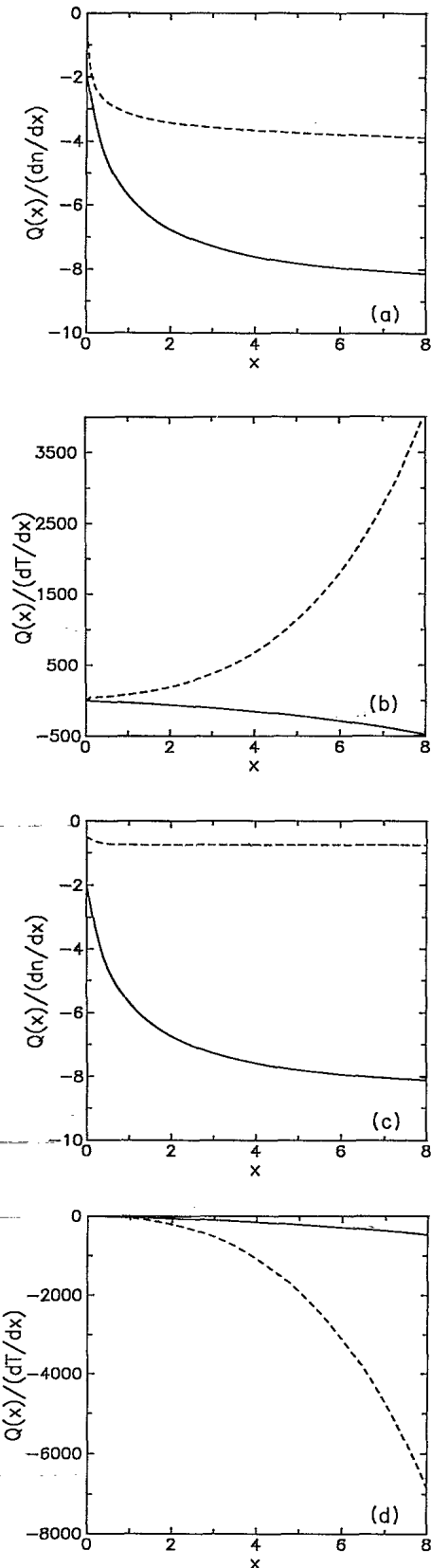


FIG. 8. Ratio of the actual heat flux  $Q(x)$  to the density gradient and the temperature gradient for the Coulomb cross section [(a) and (b)] and the hard-sphere cross section [(c) and (d)] for  $\gamma=0.01$  (solid lines) and  $\gamma=50$  (dashed lines).

mixture for which species 1 is present in large excess and acts as a thermal bath at equilibrium. This is equivalent to considering the limit in which  $n_2/n_1 \rightarrow 0$  and the distribution function of species 1 is the Maxwell-Boltzmann distribution with a constant temperature  $T_1$ . Note that, in the limit  $n_2/n_1 \rightarrow 0$ , the temperature of the mixture coincides with the temperature of the bath and is therefore constant. This is consistent with our result that the (asymptotic) heat flux is entirely due to thermal diffusion and not to heat conduction. In this limit we only consider the kinetic equation for the distribution function of

species 2 with the 1-2 collision operator and no 1-1 collisions, namely Eq. (14) (see Eq. 8.31.5.b of Ref. [17]).

The formalism for the calculation of thermal-diffusion coefficients in binary mixtures has been presented by Chapman and Cowling [17] and by Mason and co-workers [33,39]. The results of the first or higher Chapman-Enskog (CE) approximations are given in these references for arbitrary mass and density ratios. In the limit  $n_2/n_1 \rightarrow 0$ , the thermal-diffusion coefficient for the hard-sphere cross section in the first approximation is given by these authors as (see Eq. 9.83.1 of Ref. [17])

$$\kappa_{\text{asympt}} = \frac{15\sqrt{\pi}}{16} \left[ \sqrt{1+\gamma} - \frac{\gamma[2(1+\gamma)]^{3/2} - (d/d_1)^2(15-23\gamma)}{20\sqrt{2}K(\gamma)} \right] \left[ 1 + \frac{1}{\gamma} \right]^{1/2}, \tag{24}$$

where

$$K(\gamma) = \frac{13}{20}\gamma^2 + \frac{4}{5}\gamma + \frac{3}{2}, \tag{25}$$

$d = (d_1 + d_2)/2$ , with  $d_1$  and  $d_2$  the diameters of the particles of species 1 and species 2, respectively. This expression shows that, even in the limit  $n_2/n_1 \rightarrow 0$ ,  $\kappa_{\text{asympt}}$  depends on the collision cross section of the bath particles with themselves, that is 1-1 collisions. This is due to the fact that in the CE approach both species are assumed to be perturbed from thermodynamic equilibrium and the perturbation induced in the bath distribution does not vanish in the limit  $n_2/n_1 \rightarrow 0$ . Formally, this is equivalent to solving both Eqs. 8.31.5a and 8.31.5.b of Ref. [17], retaining only the 1-1 collision operator in the former and the 1-2 collision operator in the latter. This procedure is inappropriate here since we have assumed at the outset that the bath is not perturbed from a Maxwellian. We have also chosen the normalization such that the particle flux  $j(x) = \text{const} = -1$ , so that the heat flux given by the present formalism corresponds to the thermal-diffusion ratio  $\kappa = \kappa_{\text{asympt}}/D$ , where  $D$  is the diffusion coefficient. With these additional constraints, the first-order solution of Eq. 8.31.5.b of Ref. [17] gives a thermal-diffusion coefficient of the form

$$\kappa_{\text{asympt}} = \frac{45}{32} \sqrt{\pi} K_2(\gamma, C) \tag{26}$$

for the hard-sphere cross section and similarly

$$\kappa_{\text{asympt}} = \frac{45}{16} \sqrt{\pi} K_2(\gamma, C) \tag{27}$$

for the Coulomb cross section. Here,

$$K_2(\gamma, C) = \sqrt{1+1/\gamma} \frac{K(\gamma) - (C-1)\gamma(1+\gamma)/2}{K_1(\gamma, C)}, \tag{28}$$

where

$$K_1(\gamma, C) = K(\gamma) - \frac{5}{4}(C-1)^2\gamma^2 \tag{29}$$

and  $C$  is expressed in terms of integrals over the cross section (see Eqs. 9.8.7, 9.33.2, and 9.33.3 of Ref. [17]). For the hard-sphere cross section  $C = \frac{6}{5}$ , and for the Coulomb cross section  $C = \frac{2}{5}$  (in the limit of  $\ln \Lambda \gg 1$ ). It

is useful to add the results of the first-order CE calculation of the diffusion coefficient,  $D$ . For the hard-sphere cross section we have that,

$$D = \frac{9}{16} \sqrt{\pi} \sqrt{1+1/\gamma} \frac{K(\gamma)}{K_1(\gamma, C)}, \tag{30}$$

whereas for the Coulomb cross section we get that,

$$D = \frac{9}{8} \sqrt{\pi} \sqrt{1+1/\gamma} \frac{K(\gamma)}{K_1(\gamma, C)}. \tag{31}$$

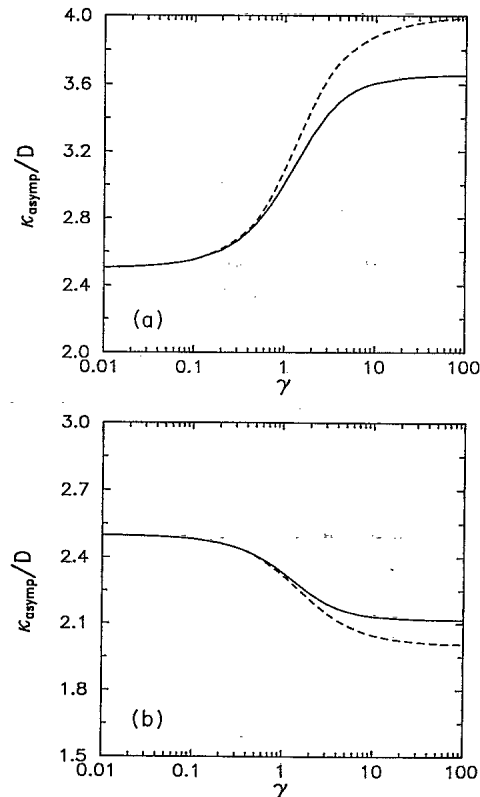


FIG. 9. Thermal-diffusion ratio  $\kappa_{\text{asympt}}/D$  as a function of  $\gamma$  for (a) the Coulomb cross section and (b) the hard-sphere cross section. Solid lines, first-order (Chapman-Enskog) approximation; dashed lines, converged numerical results with  $N=L=12$ .

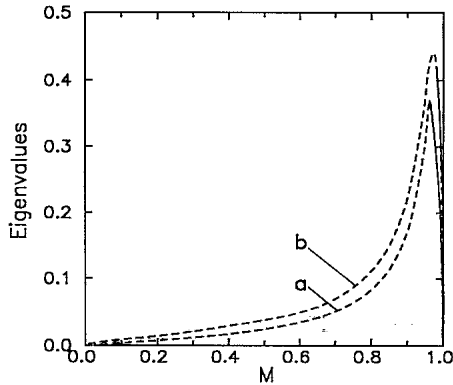


FIG. 10. Magnitude of the (curve *a*), first and (curve *b*), fourth nonzero eigenvalue as function of  $\gamma$  for the Coulomb cross section;  $N=16, L=10$ . On the dashed portion of the curves the eigenvalues have not converged.

As expected, we find exact agreement between the CE thermal-diffusion ratio and the numerical results when the expansion in Burnett functions for the numerical solution is truncated at  $L=2$  and  $N=2$ . In Figs. 9(a) and 9(b), we show the CE first approximation to the thermal-diffusion ratio  $\kappa_{\text{asympt}}/D$  (solid line) and the converged numerical result (with  $L=12$  and  $N=12$ ; dashed line) as functions of  $\gamma$  for the Coulomb and the hard-spheres cross sections, respectively. It is clear that the convergence is much faster at small  $\gamma$ , where the CE first approximation coincides with the exact results. Note that the CE approximation retains the qualitative behavior of the curve in both cases. The different functional behavior of the thermal-diffusion ratio for the two different cross sections studied can be seen analytically by differentiating  $\kappa$  with respect to  $\gamma$ . In either case we obtain

$$\frac{d\kappa}{d\gamma} = -(C-1) \left[ \frac{(1+2\gamma)K - \gamma(1+\gamma)K'}{K^2} \right]. \quad (32)$$

The factor in large parentheses is the same for the hard-sphere and the Coulomb cross sections, so the sign of the derivative is given by the factor  $C-1$ , which takes on opposite sign in the two cases.

The different qualitative behavior of the extrapolation length and the spatial variation of the density, temperature, and heat flux as functions of the mass ratio can be explained by comparing the first few eigenvalues for the Coulomb and the hard-sphere cross sections. In Fig. 10 we show the spatial eigenvalues,  $g_1$  and  $g_4$ , as functions of  $M = m_2/(m_1 + m_2) = 1/(1 + \gamma)$  for the Coulomb cross section to be compared with the corresponding results for the hard-sphere cross section in Fig. 2 of I. The solid portions of the curves in Fig. 10 correspond to eigenvalues that appear to have converged numerically whereas the dashed portions refer to unconverged values. For both cross sections, the eigenvalues rise steeply as  $\gamma$  increases from zero (i.e., the Rayleigh limit,  $M \leq 1$ ), reach a

maximum and then decay to zero as  $\gamma \rightarrow \infty$  (i.e., the Lorentz limit,  $M \rightarrow 0$ ). However, the maximum occurs at  $M=0.5$  for the hard-sphere cross section and at  $M \approx 0.97$  for the Coulomb cross section. Also, for  $M \rightarrow 0$ , the eigenvalues for the Coulomb cross section are very much smaller than the corresponding eigenvalues for the hard-sphere cross section. The explicit form of the differential Fokker-Planck collision operator as a sum of an isotropic and an anisotropic term was given by Hinton and others [19]. The ratio of the isotropic to the anisotropic contribution is of order  $(m_2/m_1)^2$ , so that in the Rayleigh limit ( $\gamma \rightarrow 0, M \rightarrow 1$ ) the scattering operator becomes isotropic. Hence, the density profiles shown in Figs. 4(c) and 4(d) in the Rayleigh limit for the two cross sections are very similar. In the Lorentz limit, since the spatial eigenvalues are smaller for the Coulomb cross section than for the hard-sphere cross section, the density profile shown in Fig. 4(a) for the Coulomb cross section approaches the asymptotic limit much more slowly than for the hard-sphere cross section [Fig. 4(b)]. Consequently, the extrapolation length is much larger for the Coulomb cross section than for the hard-sphere cross section in this mass range. The spatial variation of  $T(x)/T_1$ , shown in Figs. 6(a) and 6(b), given by Eq. (4.8) of I, is not as easily interpreted as we have done for the density profile. The overshoot of this ratio for the Coulomb cross section [curves *d-g*, Fig. 6(a)] is an interesting effect that does not occur for the hard-sphere cross section.

#### IV. SUMMARY

We have presented a numerical solution of the Boltzmann equation for the Milne problem with Coulomb scattering and compared the results with the ones obtained previously for the case of the hard-sphere cross section. The method of solution is the same as in I and consists in splitting the distribution function into transient and asymptotic portions. The transient part is important near the boundary, while far from the boundary the asymptotic or hydrodynamic solution which corresponds to the Chapman-Enskog solution of the Boltzmann equation becomes valid. The Boltzmann equation for both portions of the distribution function is solved with the expansion in Burnett functions and application of the Marshak (and variational) boundary conditions. We have studied the behavior of the extrapolation length, the diffusion coefficient and the temperature, density, and heat-flux profiles versus the mass ratio for both cross sections. The results obtained for the two cross sections appear to be very similar in the Rayleigh limit ( $\gamma \rightarrow 0$ ), where the collision operator is isotropic and of similar form for the two cross sections. By contrast, the results for the other mass ratios can be significantly different. For example, the extrapolation length for the Coulomb case exhibits a minimum at  $\gamma \approx 1$ , while in the hard-sphere case it decreases monotonically with  $\gamma$ . Also, the temperature profile near the boundary for  $\gamma \geq 1$  for the Coulomb cross section exhibits an overshoot relative to the bath temperature not observed in the hard-

sphere case. We have also discussed at length that the heat flux in this physical situation is due to thermal diffusion rather than to conduction. Finally, a qualitative explanation of the different results for the two cross sections has been provided in terms of the mass dependence of the spatial eigenvalues.

#### ACKNOWLEDGMENT

This research is supported by a grant from the Natural Science and Engineering Research Council of Canada and a grant from the Petroleum Research Fund administered by the American Chemical Society.

\*Present address: Theoretical Studies Department, Industrial Technology, B424.4 Harwell Laboratory, Oxfordshire OX11 0RA, United Kingdom.

†Also with the Department of Geophysics and Astronomy, University of British Columbia, Vancouver, British Columbia, Canada.

- [1] E. A. Milne, *Handb. Astrophys.* **3**, 1 (1930).
- [2] V. Kourganov, *Basic Methods in Transfer Problems* (Oxford University, Oxford, England, 1963).
- [3] M. M. R. Williams, *Mathematical Methods in Particle Transport Theory* (Butterworths, London, 1971); J. J. Duderstadt and W. R. Martin, *Transport Theory* (Wiley, New York, 1979); K. M. Case and P. F. Zweifel, *Linear Transport Theory* (Addison-Wesley, Reading, Mass, 1967); C. Cercignani, *The Boltzmann Equation and Its Applications* (Springer-Verlag, New York, 1988).
- [4] M. J. Lindenfeld and B. Shizgal, *Phys. Rev. A* **27**, 1657 (1983).
- [5] K. Frankowski, Z. Alterman, and C. L. Pekeris, *Phys. Fluids* **8**, 245 (1965).
- [6] S. K. Loyalka, S. A. Hamoodi, and R. V. Tompson, *Phys. Fluids A* **1**, 384 (1989).
- [7] G. I. Bell and S. Glasstone, *Nuclear Reactor Theory* (Van Nostrand Reinhold, New York, 1970).
- [8] K. Razi Naqvi, S. Waldenstrom, and K. J. Mork, *J. Chem. Phys.* **78**, 2710 (1983).
- [9] S. Waldenstrom, K. J. Mork, and R. Razi Naqvi, *Phys. Rev. A* **28**, 1659 (1983).
- [10] D. C. Sahni, *Phys. Rev. A* **30**, 2056 (1984).
- [11] K. Razi Naqvi, K. J. Mork, and S. Waldenstrom, *Phys. Rev. A* **40**, 3405 (1989).
- [12] E. A. Johnson, *J. Stat. Phys.* **37**, 647 (1989); C. J. Goebel, S. M. Harris, and E. A. Johnson, *Phys. Fluids* **19**, 627 (1976); *Rarefied Gas Dyn.* **51**, 109 (1977).
- [13] M. E. Widder and U. M. Titulaer, *J. Stat. Phys.* **55**, 1109 (1989); G. F. Hubmer and U. M. Titulaer, *ibid.* **59**, 441 (1990); **63**, 203 (1991).
- [14] A. R. Barakat and J. Lemaire, *Phys. Rev.* **42**, 3291 (1991).
- [15] B. Shizgal and R. Blackmore, *Planet. Space Sci.* **34**, 279 (1986).
- [16] H. J. Fahr and B. Shizgal, *Rev. Geophys. Space Phys.* **21**, 75 (1983).
- [17] S. Chapman and T. G. Cowling, *The Mathematical Theory of Nonuniform Gases* (Cambridge University, Cambridge, England, 1970).
- [18] L. Spitzer and R. Harm, *Phys. Rev.* **89**, 977 (1953).
- [19] E. M. Epperlein and M. G. Haines, *Phys. Fluids* **29**, 1029 (1986); F. L. Hinton, in *Handbook of Plasma Physics*, edited by M. N. Rosenbluth and R. Z. Sagdeev, *Basic Plasma Physics I* Vol. 1 (North-Holland, Amsterdam, 1983), pp. 147–197; A. R. Hochstim and G. A. Massel, in *Kinetic Processes in Gases and Plasmas*, edited by A. R. Hockstim (Academic, New York, 1969), pp. 142–255; S. I. Braginskii, in *Reviews of Plasma Physics*, edited by M. A. Leontovich (Consultants Bureau, New York, 1965), Vol. 1, pp. 205–311; J. P. Shkarofsky, I. B. Bernstein, and B. B. Robinson, *Phys. Fluids* **6**, 40 (1963).
- [20] E. Leer and T. E. Holzer, *J. Geophys. Res.* **77**, 4035 (1972); J. Lemaire and M. Scherer, *Rev. Geophys. Space Phys.* **11**, 427 (1973); E. Marsch and H. Goldstein, *J. Geophys. Res.* **88**, 9933 (1983).
- [21] R. W. Schunk, *Rev. Geophys. Space Phys.* **15**, 429 (1977).
- [22] C. E. Max, in *Laser-Plasma Interactions*, edited by R. Balian and J. C. Adam (North-Holland, Amsterdam, 1982).
- [23] G. J. Rickard, A. R. Bell, and E. M. Epperlein, *Phys. Rev. Lett.* **62**, 2687 (1989); P. A. Holstien, J. Delettrez, and S. Skupsky, *J. Appl. Phys.* **60**, 2296 (1986); G. J. Rickard, A. R. Bell, and E. M. Epperlein, *Phys. Rev. Lett.* **61**, 2453 (1983); J. F. Luciani and P. Mora, *ibid.* **51**, 1664 (1983); D. R. Gray and J. D. Kilkenny, *Plasma Physics* **22**, 81 (1980).
- [24] A. V. Phelps, *J. Res. Natl. Inst. Standards Tech.* **95**, 407 (1990); P. J. Chantry, A. V. Phelps, and G. J. Shulz, *Phys. Rev.* **152**, 81 (1966).
- [25] E. Leer, T. E. Holzer, and T. Fla, *Space Sci. Rev.* **33**, 161 (1982).
- [26] J. F. Luciani, P. Mora, and R. Pellat, *Phys. Fluids* **28**, 835 (1985).
- [27] V. V. Belyi, W. Demoulin, and I. Paiva-Veretennicoff, *Phys. Fluids B* **1**, 305 (1989); **1**, 317 (1989).
- [28] H. Grad, *Pure Appl. Math.* **2**, 325 (1949).
- [29] H. J. Fahr, *Ann. Geophys.* **32**, 277 (1976).
- [30] J. M. Burgers, *Flow Equations for Composite Gases* (Academic, New York, 1969).
- [31] N. N. Ljepojevic and P. MacNeice, *Phys. Fluids A* **40**, 981 (1989).
- [32] R. Roussel-Dupre, *Astrophys. J.* **243**, 329 (1981); **252**, 393 (1982).
- [33] L. Monchick and E. A. Mason, *Phys. Fluids* **28**, 3341 (1985).
- [34] B. Shizgal, U. Weinert, and J. Lemaire, *Rarefield Gas Dynamics 15*, edited by V. Boffi and C. Cercignani (Teubner, Stuttgart, 1986), pp. 374–383.
- [35] E. C. Shoub, *Phys. Fluids* **30**, 1340 (1987).
- [36] S. K. Wong, *Phys. Fluids* **28**, 1695 (1985).
- [37] N. Corngold, *Phys. Rev. A* **15**, 2454 (1977); **24**, 656 (1981).
- [38] B. Shizgal, *Rarefied Gas Dynamics* **17**, 22 (1991).
- [39] E. A. Mason and F. J. Smith, *J. Chem. Phys.* **44**, 3100 (1966); E. A. Mason, R. J. Munn, and F. J. Smith, in *Advances in Atomic and Molecular Physics*, edited by D. R. Bates and I. Estermann (Academic, New York, 1966), Vol. 2, Sec. 2; L. Monchick, S. I. Sandler, and E. A. Mason, *J. Chem. Phys.* **49**, 1178 (1968).